ANYexo: A Versatile and Dynamic Upper-Limb Rehabilitation Robot

Author(s):
Zimmermann, Yves; Forino, Alessandro; Riener, Robert; Hutter, Marco

Publication date:
2019-10

Permanent link:
https://doi.org/10.3929/ethz-b-000356123

Originally published in:
IEEE Robotics and Automation Letters 4(4), https://doi.org/10.1109/LRA.2019.2926958

ANYexo: A Versatile and Dynamic Upper-Limb Rehabilitation Robot

Yves Zimmermann[1,2], Alessandro Forino[1], Robert Riener[2,*], and Marco Hutter[1,*]

***Abstract*—This paper presents a versatile upper-limb exoskeleton based on low-impedance torque controllable series elastic actuators. This experimental platform is designed to validate novel algorithms and hardware concepts for more autonomous therapy of moderately and severely affected patients with a neural impairment. The design is optimized to achieve a large range of motion (ROM) and robust interaction force control to best mimic the compliant and accurate haptic interaction of therapists. The presented robot covers the relevant ROM required for activities of daily life (ADL) particularly including poses close to the torso, head, and behind the back. The kinematics are optimized for high manipulability during ADL and low inertia. We use modified modular series elastic actuators that provide the required power and torque control performance. We demonstrate highly transparent behavior up to speeds of $11\,\mathrm{rad/s}$ with a feed-forward torque controller based on an accurate dynamic model. The presented robot unites a large ROM with optimized manipulability, high nominal power to weight ratio ($111\,\mathrm{W/kg}$), accurate torque control at speeds sufficient for unconstrained recovery of patients, and versatility for a broad variety of experiments in one device. To our knowledge, no other device is tailored to such an extent for this application.**

***Index Terms*—Rehabilitation Robotics, Physical Human-Robot Interaction, Physically Assistive Devices**

I. Introduction

IMPAIRMENT of the central nervous system is a common cause for the loss of motor functions in adults. For most patients, there is a chance to at least partially recover the lost motor function with movement therapy [1]. Studies indicated that a significantly higher amount of therapy than provided nowadays would be beneficial [2].

Much research effort in rehabilitation robotics was dedicated to relieve therapists of the physical workload and to investigate novel therapy tools (e.g. virtual reality, adaptive assistance strategies) [3], [4]. Multiple studies indicated the applicability of these devices and could show a significant benefit regarding the therapy outcome [5], [6]. The cost of robotic therapy is still slightly higher than for conventional therapy [7]. This is partially caused by the commonly used one-to-one setting of patient and therapist in training sessions. However, autonomous robot-assisted therapy for severely and moderately affected patients was not much addressed despite the large anticipated potential.

Fig. 1. Exoskeleton arm of ANYexo with a user.

We strive for more autonomy of rehabilitation robots designed for said patient group. Therefore, this new generation should be able to mimic the sensitive and nimble haptic interaction of therapists with minimum hardware complexity. We aim for a ROM large enough for most ADL which further reduces the need for therapy without robots. Movements close to the body are particularly included to account for training of ADL comprising interaction with other body parts and strongly shortened postures. The robot presented in this paper is designed as an experimental platform to validate novel control methods and hardware concepts to achieve this research goal. The resulting design is shown in Fig. 1.

For severely and moderately affected patients all DoF of the affected arm should be controlled to avoid and train against pathological synergies. Therefore, a robot with exoskeleton structure is most suitable. A broad variety of exoskeletons for rehabilitation was developed [3]. Only a few of them fully actuate the shoulder joints. Some examples show a passive compensation mechanism for the shoulder girdle DoF [8]. Others approximate the scapulohumeral rhythm by mechanically coupling the translation of the glenohumeral joint to its rotation [9]. However, the active assistance of the scapulohumeral rhythm by an impedance controller can reduce the undesired interaction forces remarkably [10].

High quality of interaction force control was achieved by [10] and [11]. Exoskeletons should correct pathological synergies without constraining the patients. Hence, haptic transparency is required for movements faster than the ones in ADL [12] to allow for unlimited recovery of motor functions. This is not possible with the devices in [10], [11]. For assessments of reflex properties of patient arms, high force

Manuscript received: February, 24, 2019; Revised: May, 10, 2019; Accepted: June, 11, 2019.

This paper was recommended for publication by Editor Pietro Valdastri upon evaluation of the Associate Editor and Reviewers' comments. This work was supported by ETH funds and NCCR Robotics.

[1] First, second, and last author are with Robotic Systems Lab, ETH Zurich, Switzerland yvesz@ethz.ch

[2] First and second last author are with Sensory-Motor Systems Lab, ETH Zurich, Switzerland. Second last author is additionally with Spinal Cord Injury Center, University Hospital Balgrist, Zurich, Switzerland riener@ethz.ch.

* Second last and last author contributed to equal parts to the lead of this project.

Digital Object Identifier (DOI): see top of this page.

control bandwidths are necessary [8].

Torque controlled joints are beneficial to achieve a high quality of interaction force control [13]. Hence, series elastic actuation is well suited for rehabilitation robots [14]. A recent implementation of hydraulic SEA in rehabilitation robots is shown by [8]. They achieve a high force control bandwidth exceeding the force control bandwidth of the human which is $\approx$5 Hz to 10 Hz by a magnitude [15]. Another recent SEA driven exoskeleton is presented by [10] which uses electric actuation achieving a force control bandwidth of 7 Hz at an unknown amplitude.

In chapter II we will explain the kinematics, link, and actuation design. In chapter III we present the implemented software structure and controllers and in chapter IV we show the performance of the system with some experiments.

II. System Design

The main goal for the presented robot is to serve as a test-bed to investigate novel control methods based on torque control for high fidelity interaction force tracking. Further, we intend to make statements regarding recommended trade-offs in competing design goals possible (*e.g.* cost vs. DoF, instrumentation vs. weight). Therefore, the robot's design should strive to reach the maximum reasonable performance while being versatile to simulate these trade-offs. Hence, these aspects together with a large ROM and lightweight design were more prioritized than admissibility for medical device certificates, maintenance, and cost. The targeted patient group is moderately to severely affected. In this paper, we will refer to the person strapped to the exoskeleton structure as *patient* and the person interacting with the device from the outside as *therapist*.

A. Requirements

The device should cover as much of the ROM used in ADL as possible without accepting an unreasonable increase in robot inertia. The ROM required for ADL by 95 % of the population was derived from the maximum values of the related work in [16], [17], [18] and translated to the ISB system [19]. For severely affected patients, the device should be strong enough to move a passive human arm. Free space rendering up to speeds at least double the required speed in ADL should be possible to avoid limiting the movement capability of moderately affected patients. The maximum speeds and torques required in ADL are taken from [12]. The values for PoE and AoE are defined as the largest value of the x- and y-axes in [12]. As strength training and assessment are an essential part of the therapy, we strive to cover the average maximum force of the male and female population investigated in [20]. The reference values for mentioned requirements are shown in Tab. I. All DoF of the exoskeleton should be actuated or fixed during operation to allow full control over the systems dynamics. Further, the actuators of the exoskeleton should perform such, that they can be assumed as perfect torque sources in the relevant frequency range. The human torque control bandwidth was found to be $\approx$5 Hz to 10 Hz by [15]. We strive for a torque control bandwidth that is approximately a magnitude higher to achieve an indulgent control behavior in tracking human like torque profiles. To investigate different training poses and torso alignment strategies we want the device to be usable with standard, fixed and wheeled chairs as well as in standing position. The device is designed to be adjustable to the size of the 5$^{\text{th}}$-percentile female to 95$^{\text{th}}$-percentile male. As this device is dedicated for experimental purpose, we sacrifice left arm usage for a simpler and more lightweight design. Many of the planned investigations with the device are feasible with the proximal DoF *i.e.*, shoulder and elbow. Hence, the development of an actuated forearm, wrist and hand module of the exoskeleton is delayed. Therapists must be able to stand close to the patients affected arm and interact haptically with the exoskeleton structure. An overview of the system's components is given in Fig. 2.

DOF	ROM [16], [17], [18]	speed [12]	torque ADL [12]	torque max [20]
unit	°	°/s	N m	N m
min. PoE	-87.4	172	10	54
max. PoE	116.8	172	10	54
min. AoE	0	172	10	54
max. AoE	128	172	10	54
max. ext. IER	94	141	3	31
max. int. IER	132	141	3	31
max. EFE	143	173	4	55

TABLE I
Reference ROM, joint speed, and torque in ISB coordinates [19]: Plane of Elevation (PoE), Angle of Elevation (AoE), internal/external Rotation (IER), and elbow flexion/extension (EFE).

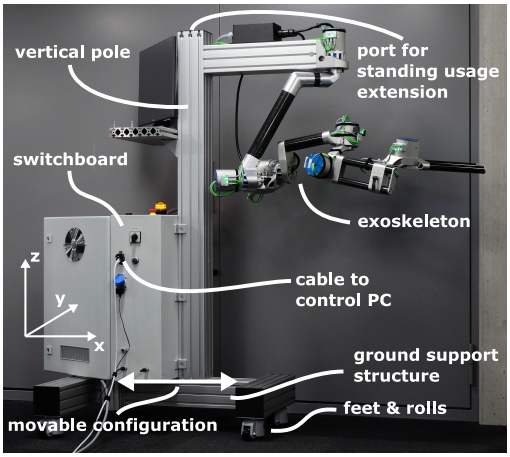

Fig. 2. System overview in the configuration for use with a regular chair.

B. Kinematics

An exoskeleton has to be aligned to the human joint axes as accurate as possible. Uncontrolled DoF to align the joints as used in [8] are not admissible as we require full controllability of the exoskeletons dynamics. The Glenohumeral joint (GH) itself can be modeled as a spherical joint. However, the scapulohumeral rhythm couples the joint angles of the GH joint with the movement of the shoulder girdle (SG) elevation/depression (GED) and protraction/retraction (GPR) movement. Actuated shoulder girdle DoF as used by [10] have shown superior performance regarding parasitic interaction forces compared to a mechanical coupling [9], [21]. Hence, we include the

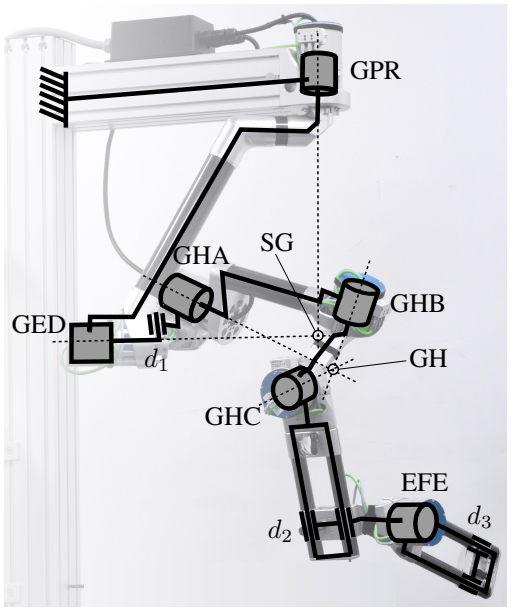

Fig. 3. The kinematic structure of the robot with the shoulder girdle joints (SG): protraction/retraction (GPR) and elevation/depression (GED); the glenohumeral joints (GH): GHA, GHB, and GHC; elbow joint EFE; fixed passive link length adjustments d_i.

two main shoulder girdle DoF as active joints. The resulting kinematic structure is shown in Fig. 3. The exoskeleton is adjusted to a patient starting by the alignment of the SG joint by placement of the chair and height of the exoskeleton. The width of the shoulder and the lengths of upper arm, forearm, and hand are then adjusted by the prismatic joints d_i which are fixed during operation. The joint and link length alignment happens from proximal to distal using palpation and visual inspection. The structure is designed such, that the exoskeleton can be attached to a patient even in the typical shortened pose. The torso could be fixed to a backrest mounted on the base using a harness. The following sections describe how the kinematics of the GH and SG joints were developed. The elbow joint (EFE) does not need more explanation, as it is a simple monocentric joint.

1) Shoulder Girdle (SG): The exoskeleton was developed using the human model in Siemens NX with the ANSUR anthropometric data. The whole assembly of the exoskeleton is constrained to this human model which has protraction/retraction and elevation/depression axes that intersect. This does not correspond to the findings of [10] which did an experiment with one healthy subject and found a distance of $24\,\mathrm{mm}$ between the two SG axes. However, the translational trajectories of the GH joint of these two models deviate only $<3\,\mathrm{mm}$. Therefore, we decided to rely on the ANSUR based human model without further investigations. The robot's SG axes are chosen such that they act on protraction/retraction and elevation/depression in a decoupled manner. The ranges are restricted to $-14°$ to $31°$ for the GPR and $-24°$ to $32°$ for GED respectively using the same sign convention as ISB.

2) Glenohumeral Joint (GH): The GH joint of an exoskeleton is challenging as the joints and actuators should be located as close to the rotation center as possible to keep the reflected inertia at the joints small. Simultaneously, collisions with the head, torso, and arm of the patient must be avoided. Additionally, the configuration of the rotation axes influences the manipulability of the humerus orientation μ_{humerus} defined as the product of the singular values σ_i of the rotation Jacobian of the humerus

$$\mu_{\text{humerus}} = \prod_i \sigma_i \in [0, 1]. \tag{1}$$

When all three axes are perpendicular $\mu = 1$ and in the case where two of the robot axes coincide, the humerus cannot rotate anymore in one of the three directions and $\mu = 0$. The glenohumeral joint of exoskeletons is often designed such that the third joint coincides with the internal/external rotation axis (IER). The technical solutions of this approach are usually bulky and prevent a ROM close to the body. Another approach is to choose the orientation of the axes in a way that simple monocentric joints can be used as it is shown *e.g.* for Harmony in [10]. Compared to Harmony we do not have to consider the bimanual ROM, hence have more freedom to place the axes.

The goal of the kinematic design is to achieve an exoskeleton-ROM that covers as much of the ADL-ROM as possible while providing an optimal manipulability within this ROM. Manipulability is closely related to the achievable transparency as it describes how well the humerus orientation is controllable by the actuators. We choose the three axes to be orthogonal in the zero-configuration to maximize the manipulability. Further, we determine the main axis of the humerus to coincide with the first GH-axis (GHA) in the zero-configuration as shown in Fig. 4c). By this constraint, we place all singular orientations of the humerus ($\mu = 0$) to be perpendicular to the GHA axis. At the same time, the GHA axis marks now the direction where the humerus has full manipulability. The angles α and β which determine the orientation of GHA can be chosen such that the maximum manipulability lies in the center of the ADL-ROM. In the final kinematics of ANYexo, the angles were chosen to be $\alpha = 40°$ and $\beta = 10°$ as shown in Fig. 4a)&b) to avoid collisions which would reduce the ROM. Still, the ADL-ROM is never perpendicular to the GHA axis, hence there are no singularities in the desired ROM. Next, the rotation γ of the two remaining axes w.r.t. the elbow joint axis has to be determined. This angle defines where the relevant singularities are located on the boundary of the hemisphere around GHA. The angle was tuned as a trade-off between maximizing the ROM by avoiding collisions and placing the weak manipulability where it least disturbs according to therapists. In Fig. 4d) the manipulability distribution for the human ROM of internal/external rotation is plotted for the final design with $\gamma = 80°$.

C. Hardware

The hardware concept of this robot is optimized regarding the anticipated control strategies that should be developed while taking the safety concerns for therapists and patients into account.

1) Actuation: The actuation system of this robot should provide accurate torque control with high robustness regarding disturbances induced by the human. Series elastic actuators were found to suit this application the best considering

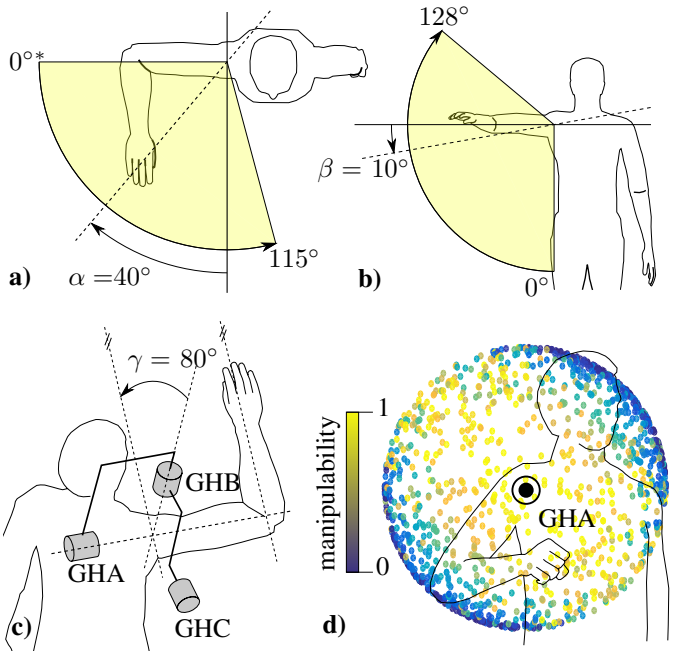

Fig. 4. a,b) orientation of the GHA axis w.r.t. the ROM for ADL [16]; c) orientation of the GHB and GHC axes; d) manipulability distribution when POE and AOE are varied by ±90° around the GHA axis and the IER is varied from 0° to 90°. *: POE <0° are barely used.

the torque requirements, aspirations for lightweight design, footprint restrictions, and rather low requirements regarding the position control performance [14], [22]. We decided for electric actuation as the communication and power cables are less stiff than hydraulic tubes resulting in less disturbance of the joint torques. The actuation must deliver sufficient torque to move a passive human arm and to compensate the robot's dynamics. The modular SEA ANYdrive developed earlier in our group [23], [24], covers the minimum requirements on torque for all joints while not exceeding the target for strength assessment. This drive can provide $40\,\mathrm{N\,m}$ peak torque at a bandwidth of $>60\,\mathrm{Hz@3\,N\,m}$ amplitude and a joint torque resolution of $<0.1\,\mathrm{N\,m}$. The maximum joint speed of $12\,\mathrm{rad/s}$ provides approximately 4-times higher speeds as usually required in ADL [12]. This increases the versatility by enabling motor learning studies with healthy people. Drives that will provide $80\,\mathrm{N\,m}$ peak torque at $6\,\mathrm{rad/s}$ maximum speed are currently in development. These would allow incorporating maximum force assessments and strength training. The robots links are designed such that both versions of the drive can be mounted. These drives can be operated in joint position, velocity, or torque control mode. These control cycles run on $2.5\,\mathrm{kHz}$ while the motor controllers are running at $10\,\mathrm{kHz}$. Limits for position, velocity, and torque can be set for safety purposes.

2) Links: All link elements of the arm were developed for high stiffness, low weight, and a maximum joint torque of $80\,\mathrm{N\,m}$. The double CFRP tube rail design with aluminum clamps shown in Fig. 1 is used at the upper arm and forearm links to be lightweight, adjustable in length, and versatile regarding the positioning of the cuffs and auxiliary tool mounting. M4 threads and $3\,\mathrm{mm}$ dowel holes in most of the aluminum link parts can be used for *e.g.* additional instrumentation. The ANYdrives only withstand bending moments up to $120\,\mathrm{N\,m}$. Therefore, a modular support bearing system was designed to hold bending moments up to $290\,\mathrm{Nm}$ required in the three proximal joints. To keep maximum modularity, we designed the mounting interface of the bearing module in the same way as the ANYdrive. The actuator locations and link shapes were designed to minimize the reflected inertia at the joints and maximize the ROM while avoiding collisions with the human. The base is built using standard *item* aluminum profiles. The anterior/posterior position of the vertical pole of the base can be shifted in a range of $0.58\,\mathrm{m}$ with respect to the ground support structure. This enables to provide an optimal support polygon location for use with wheelchairs, fixed and regular chairs as well as in standing operation (see Fig. 2). For the use in standing operation, the vertical pole is extended. The cabling for actuators and instrumentation is routed through the CFRP tubes and hollow shafts of the drives.

3) Sensory System & Mechatronic Layout: A Lenovo P51 with a Linux operating system is used as a control PC. The control PC interfaces to the hardware by EtherCAT communication. Two 6-DoF F/T-sensors Rokubi Mini 1.1 are placed between the exoskeleton and the cuffs. They measure a force and torque range of $1000\,\mathrm{N}$ and $8\,\mathrm{N\,m}$ in the z-direction and $500\,\mathrm{N}$ and $5\,\mathrm{N\,m}$ in the xy-plane with $<0.02\,\%$ noise. The actuators and FT-sensors are each equipped with an IMU. A Beckhoff PLC (CX8190) with TwinSave terminals is used for communication with analog devices like the power electronics and dead man's switches. The algorithms on the control PC can run at up to $1\,\mathrm{kHz}$.

D. Safety Concept

A 4-layer safety cascade using the high-level controller, motor controllers, and mechanical structure protects the patient from over-extension. The link design prevents to clamp fingers and is mostly based on rounded geometries, which allows the therapist to touch the exoskeleton at all links. Collisions with the patient's body can be prevented by defining task space limits on the system level controller.

III. Software

The architecture of the software framework and its interaction with hardware and humans is shown in Fig. 5. The code is mostly written in C++ as nodes for the robot operating system (ROS). A modular structure allows to adapt and exchange code efficiently with other robotic projects in our and other groups which contributes to the versatility of the device.

A. Modelling

A precise model of the robot's kinematics and dynamics is needed for the model-based control algorithms presented in section III-B. Particularly, the inverse dynamics based control approaches are very sensitive to modeling errors of the inertial terms. The robot model used for control is currently fully based on the CAD model. To guarantee a high quality of the kinematic properties CNC machined scaffolds were used for the bonding. As the part weight of each manufactured part

in CAD deviates less than $4\,\%$ from the real part weight, the density of the parts in CAD was not corrected. A parameter identification on the real system was deliberately omitted to keep the model physically meaningful. The robot model is described in URDF files which are used by the model-based control and for the physics simulation. For an initial guess of the human's link length, data from anthropometric tables is used [25]. The dynamic interaction of the simulated human and robot is described by

$$\boldsymbol{M}_i\ddot{\boldsymbol{q}}_i + \boldsymbol{h}_i(\boldsymbol{q}_i, \dot{\boldsymbol{q}}_i) + \boldsymbol{g}_i = \boldsymbol{J}_{c,i}^{\top}\boldsymbol{\lambda}_c + \boldsymbol{\tau}_i \quad i \in \{R, H\}, \tag{2}$$

where R and H are indices for the robot and human system respectively, $\boldsymbol{M}$ is the mass matrix, $\boldsymbol{h}$ the gyro and Coriolis terms, $\boldsymbol{g}$ the gravitation terms, $\boldsymbol{J}_c$ the stacked spatial Jacobian of the interaction points, $\boldsymbol{\tau}$ the joint torques, and $\boldsymbol{\lambda}_c$ the interaction wrench described by

$$\boldsymbol{\lambda}_c = f_c(\boldsymbol{q}_R, \dot{\boldsymbol{q}}_R, \ddot{\boldsymbol{q}}_R, \boldsymbol{q}_H, \dot{\boldsymbol{q}}_H, \ddot{\boldsymbol{q}}_H). \tag{3}$$

Where f can be an arbitrary function describing the interaction wrench depending on the relative motion of the interaction points. We found that a spring-damper model works well. For the high level control design, the actuators can be considered as perfect torque or position source within the bandwidths typical for humans ($\approx$7 Hz [15]).

B. Controls

A low-impedance torque controlled system best emulates the interaction of a therapist with the patient's arm. Compared to a joint position controlled approach, joint torque control allows for compliance to voluntary and non-voluntary deviations of the patient from a nominal path. Controllers that assist the patient against gravity or correct pathological synergies without a nominal path are also best realized with joint torque control.

In real therapy applications, multiple tasks and limitations are demanded at different priorities such as interaction wrench tracking, end-effector pose control and workspace limitations in joint and task space. Autonomous training requires to handle the priorities and different task types compactly and cleanly. We propose to use a *Hierarchical Optimisation Controller* which is often used for legged robots *e.g.* in [26]. The flowchart of the high-level controller using this controller is shown in Fig. 5.

This method optimizes a state vector $\boldsymbol{\xi}$ of the system to fulfill tasks defined on different priorities p, while not violating the tasks on higher priorities. On each priority the sub-tasks $\mathcal{T}_{p,i}$ can be set as equality constraints $b_i = \boldsymbol{A}_i\boldsymbol{\xi}$ or as inequality constraints $c_i - \boldsymbol{D}_i\boldsymbol{\xi} < \gamma_i$. The optimization for one priority level p is realized by solving the quadratic program (QP) defined by the stacked tasks of this priority $\mathcal{T}_p$ in the null-space $\mathcal{N}_p$ of the higher priority tasks as described in [26]. The slack variables γ_i provide numerical stability when the inequality constraint cannot be satisfied.

In our implementation, the task generation class uses the priorities as follows. *First priority* tasks are defined by the equality and inequality constraints of the physical system. This contains the equations of motion (EoM) and joint space

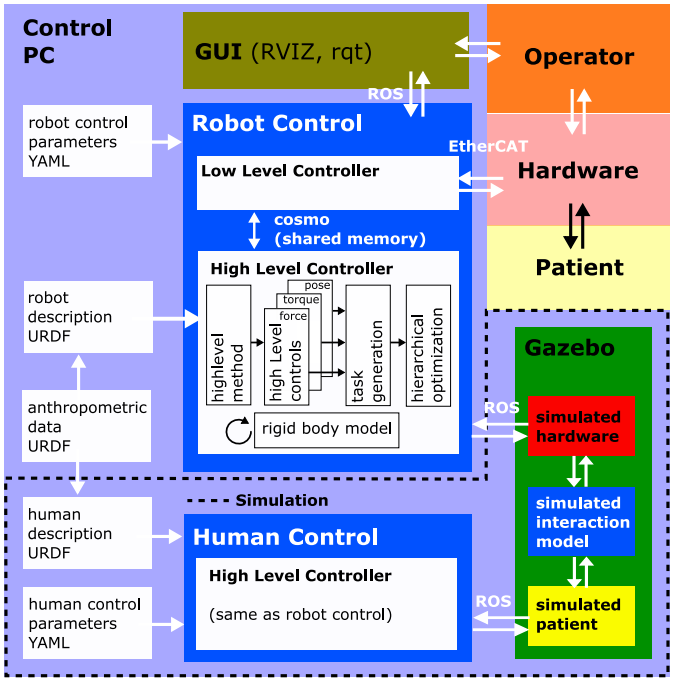

Fig. 5. Flow chart of the control structure including the simulation.

constraints in position, velocity, and torque. *Second priority* tasks contain the inequality constraints related to safety-relevant aspects as joint or task space position constraints. *Third and lower priority* are used to set the tasks defined by the high-level controls. These can be equality and inequality tasks in joint space acceleration, joint torque, or task space acceleration. The *last priority task* is used to set $\ddot{\boldsymbol{q}}_{\text{des}} = \boldsymbol{0}$ such that in case of an underdetermined system a solution without joint acceleration is preferred. The optimal joint torque $\boldsymbol{\tau}^*$ resulting from the hierarchical optimization is used as reference torque for the actuators.

A simple controller for transparent behavior is achieved by setting the interaction wrench in the EoM task to zero and further only set the zero-acceleration task. As long as the physical and safety related limits are not active this controller behaves the same as a feed-forward compensation of the systems dynamics

$$\boldsymbol{\tau}_{\text{ff}} = \boldsymbol{h}(\boldsymbol{q}_{\text{current}}, \dot{\boldsymbol{q}}_{\text{current}}) + \boldsymbol{g}(\boldsymbol{q}_{\text{current}}). \tag{4}$$

Equality tasks for interaction wrench tracking can be set at any priority if we use the full optimization vector

$$\boldsymbol{\xi} = \begin{bmatrix}\ddot{\boldsymbol{q}}^{\top} & \boldsymbol{\tau}^{\top} & \boldsymbol{\lambda}_{\text{c}}^{\top}\end{bmatrix}^{\top}. \tag{5}$$

However, the EoM would describe the system dynamics with the desired interaction forces. This can lead to a relevant discrepancy w.r.t. the real instantaneous dynamics if the impedance of the connected system is low. Humans often behave like a low impedance while high impedance foot holds are usually assumed for legged robots [26]. We suggest to use the measured interaction wrench $\boldsymbol{\lambda}_{\text{c,meas}}$ in the EoM task, as it best describes the instantaneous dynamics of the robot. With this method the highly non-linear robot dynamics are input/output linearized by the EoM task. This linearization allows the design of interaction wrench, velocity, or position

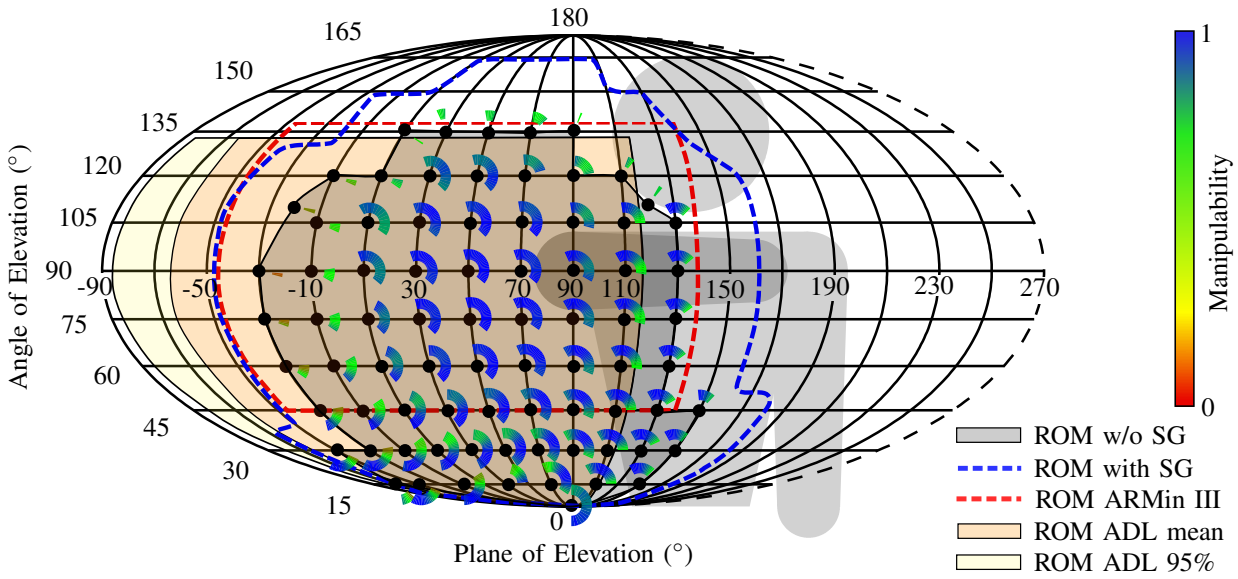

Fig. 6. The range of motion of ANYexo without SG joints is shown by the black dots in POE and AOE. The pitch circles represent the IER range and the manipulability μ_{humerus} by the color. For comparison the full ROM of the humerus in ANYexo including the SG joints, the ROM of ARMin and the mean and 95 % ROM for ADL are displayed as contours without IER information. For the ADL-ROM only the extremal values are known. The real coupled ROM for ADL is smaller, please refer to the literature [16], [17], [18]. The visualization method recommended by [27] was used.

tracking controllers using linear controls theory. The outputs of these controllers are defined as acceleration tasks in the hierarchical optimization. As the interaction wrenches are not part of the optimization anymore, it is admissible to use a reduced optimization vector $\bar{\boldsymbol{\xi}} = \begin{bmatrix}\ddot{\boldsymbol{q}}^\top & \boldsymbol{\tau}^\top\end{bmatrix}^\top$ to reduce the computational cost.

ISB DOF	ADL	ANYexo	ARMin III	Harmony
min. AoE	0	0	46	0
max. AoE	128	180	140	170
max. int. IER	-132*	-105*	-91	-89
max. ext. IER	94	105	92	79
max. EFE	143	145	123	150

TABLE II
COMPARISON ADL-ROM VS. MAXIMUM EXOSKELETON ROMS IN DEGREES. * ONLY AT LOW AOE AND POE ANGLES.

C. Simulation

The physics simulation framework Gazebo is used to simulate the full rigid body dynamics of the robot. This allows to tune and validate new controllers before testing them on the hardware. Most of the control algorithms for this device are developed for interaction with a human. Therefore we implemented a human arm in the simulation. It is modeled as a series kinematics structure using a spring-damper model for the interaction wrenches. The robot high-level control can be switched to run with the simulation environment or the hardware without any changes.

IV. EXPERIMENTS AND RESULTS

In this chapter, we present the quantitative results of the robot's design. Additionally, we describe some experiments that were conducted to assess the performance of the proposed hardware and controls.

a) Achieved ROM and Manipulability: For the safety of the patient, the ROM of the exoskeleton is restricted by mechanical end stops on the joints that prevent exceeding the maximum ROM of a healthy person. The resulting coupled three dimensional ROM and the manipulability of the shoulder joint with fixed SG are shown in Fig. 6. The ADL-ROM and ROM of ARMin are shown for comparison. The complete ROM and manipulability of ANYexo are approximated by expanding the values achieved with the fixed SG joints by the range of the SG joints. The maximum ROM values for AOE and IER are compared to Harmony [10], ARMin [9], and the ADL-ROM from the requirements in Tab. II. The ROM for ADL is covered except for large negative PoE which are only required for perineal care at small AOE to incorporate 95 % of the population [16], [17]. The mean negative PoE needed according to [17] is $-67.2°$ which is covered by ANYexo for AOE $<30°$. A 1.8 m tall healthy male strapped to the robot can reach with the hand both shoulders, the whole head, the front of the torso, both knees, right trousers pocket, and the lower back as shown in the attached video[1]. This allows training of most ADL.

b) Accuracy of the Kinematic Model: The kinematic model of the robot and joint angle calibration were validated by constraining a point on the end-effector to a linear motion w.r.t. the base. The end-effector was manually dragged along a linear guide with the robot behaving transparent using the controller described in equation (4). This experiment was done for motions in the z-direction and in the yz- and xy-plane over a distance of 0.76 m, 0.39 m, and 0.72 m. The maximum deviation from a fitted line was 4 mm, 2 mm, and 4 mm respectively. The improvised guiding structure used for this experiment had a play of 1.5 mm. This accuracy suffices for the applications in therapy.

c) Structure: The movable part of the device weights 12.98 kg with 240/720 W nominal respectively peak power

[1] https://youtu.be/F1zXnPDfTgM

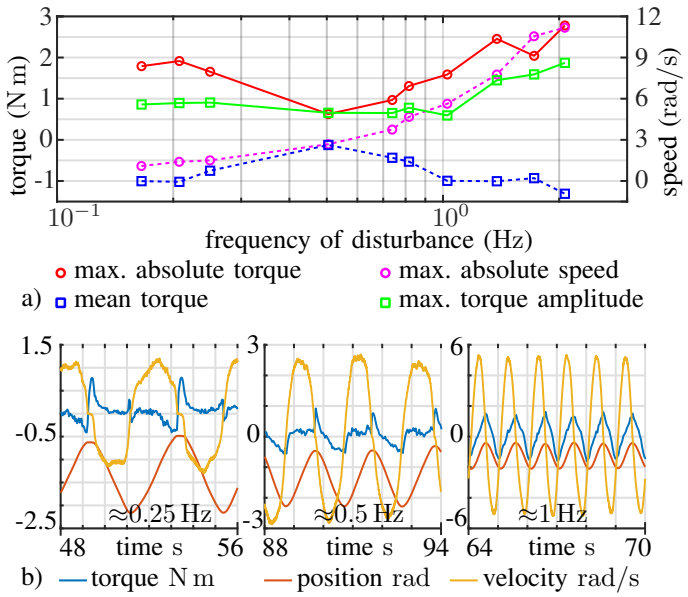

Fig. 7. a) Projected interaction torque characteristics at EFE for sinusoidal disturbance at different frequencies (evaluated over at least 4 cycles). b) reflected interaction torque at forearm during disturbances by the human.

joint	D=0.3 m	D=0.5 m	D=0.88 m
GPR	1.38	2.28	8.9
GED	4.48	6.89	7.74
GHA	4.19	2.89	12.51
GHB	1.03	0.91	4.8
GHC	1.72	3.05	3.4
EFE	2.16	2.61	4.51

TABLE III
MAXIMUM PROJECTED JOINT TORQUE IN N m CAUSED BY THE INTERACTION WRENCHES IN TRANSPARENT MODE OF THE EXOSKELETON AT DIFFERENT CIRCLE DIAMETERS D.

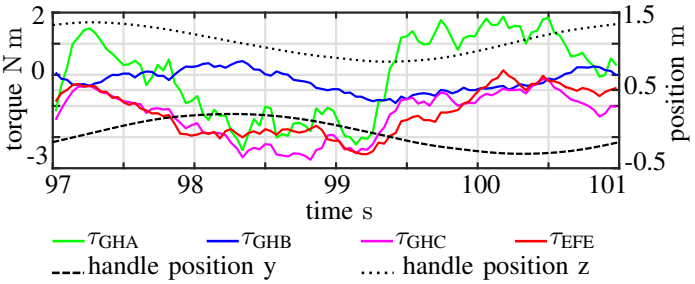

Fig. 8. Reflected interaction torques during end-effector motion on a D=0.5 m circle in the coronal plane.

per joint. ARMin V (successor of [9]) has a moving mass weight of 20.57 kg and a total nominal joint power of 509 W. Thereby, our design achieves more than 4-times higher nominal power to weight ratio than ARMin V. To our knowledge, this metric is the most suitable to compare the "lightweightness" of robots with different actuated joints. The bimanual SEA based exoskeleton Harmony weights 15.6 kg per arm. A comparison with the latter robot is difficult as the nominal power of the actuators is not known and it has one DoF more than the ANYexo.

d) Transparency: A common metric for the force control fidelity of robots in interaction with humans is transparent haptic behavior as desired forces can easily be added on top [11]. We investigated the transparency of the robot using the feed-forward joint torque controller described by equation (4). For the experiments a healthy person was attached to the robot to induce the disturbance. The characteristics of the transparency regarding the disturbance's frequency was investigated by sinusoidal motions of the forearm at amplitudes $>40°$ at different frequencies in the range of 0.17 Hz to 2.07 Hz. The projected interaction torque response at EFE is shown in Fig. 7a) with the maximum absolute value, mean, and maximum amplitude. At the frequency of ≈2 Hz joint speeds >11 rad/s were achieved. Some of the trajectories from the experiments are shown in Fig. 7b). To investigate the transparency during motions of the whole arm we project the interaction wrench of both interaction points to the corresponding torques at the joints $\boldsymbol{\tau}_{\text{proj}} = \boldsymbol{J}_{\text{UA}}^T \boldsymbol{\lambda}_{\text{UA}} + \boldsymbol{J}_{\text{FA}}^T \boldsymbol{\lambda}_{\text{FA}}$. The test subject was asked to track circles of different size in the coronal plane at height of the chest in a frequency of 0.25 Hz which was chosen equal to the "quick" setting in [11]. The motion was repeated until the circles could be tracked well. The results are shown in Tab. III evaluated over 4 subsequent circles and in Fig. 8. Comparing the results for the circle with 0.30 m diameter by taking the average of the maximum projected GH joint torques we achieve a similar transparency with only the feed forward controller on ANYexo 2.31 N m as with the disturbance observer on ARMin 2.30 N m [11].

The achieved ROM, transparency and collision avoidance are further demonstrated in the attached video.

V. DISCUSSION AND CONCLUSION

In this paper, we presented a novel shoulder and arm exoskeleton robot. This device is optimized to serve as a research platform for the development of control algorithms and hardware concepts for robot-assisted therapy of moderately to severely affected patients. The goal was to design a robot that can behave highly transparent even at healthy speeds of the arm, can cover the relevant part of the ROM required for ADL, and is highly versatile to allow for a broad variety of control and hardware experiments. We developed a shoulder kinematic that covers the desired ROM. Compared to ARMin [9] our design also includes the ROM at angles of elevation lower than 45° as well as close to the torso which is important for ADL. Due to collisions between the last shoulder link and the chest of patients ARMin does not allow POE angles larger than 90° for many patients. ANYexo has an optimized placement of the manipulability for training ADL while the kinematics of Harmony [10] are optimized for the bi-manual design more than manipulability. ANYexo achieves maximum manipulability in the center of the ADL-ROM while Harmony has a non-orthogonal design of the glenohumeral kinematics which lowers the maximum manipulability.

The actuation system provides the required joint speeds and torque control fidelity to render high-quality free space motions. Therefore, moderately affected patients should not be limited in recovery. Furthermore, motor learning studies with healthy subjects are made possible to gain more insight in neuroplastic mechanisms. Our robot's kinematics are fully defined, which allows to control/compensate the whole robot dynamics. However, we rely on accurate alignment of the

robot to the patient compared to robots with passive DoF as LIMPACT [8]. We suggested using hierarchical optimization for rehabilitation exoskeletons. This allows handling a large number of tasks in a clean way. To our knowledge, this was not yet done. The experiments have shown that a high quality of transparency can be achieved with only a model based feed-forward controller even at high speeds. This was achieved due to the lightweight structure, accurate dynamic model, optimized manipulability, and high torque control performance of the actuators. By the lightweight and versatile design of the links, the robot is prepared for the validation of a broad variety of hardware concepts to determine the recommended trade-offs for the future generation of rehabilitation robots. To our knowledge, this device is the first to unite these attributes which makes it the best choice for the planned investigations. The presented exoskeleton enables the research for a future generation of more autonomous and highly dynamic rehabilitation robots.

In future work, we strive to achieve a better interaction force tracking performance by using feedback control. An extension with actuated forearm, wrist and hand joints is planned. The stronger drives which are in development will allow performing strength assessments and training while still providing double the speed needed for ADL.

VI. Acknowledgement

We would like to thank Farbod Farshidian, Dhionis Sako, Konrad Meyer, Elisabeth Wilhelm, Fabian Just, Klajd Lika, Emek Barış Küçüktabak, Markus Stäuble, and others from the staff of the Robotic Systems Lab and Sensory-Motor Systems Lab for their support and inputs given to the project.

References

[1] L. H. Thomas, B. French, J. Coupe, N. McMahon, L. Connell, J. Harrison, C. J. Sutton, S. Tishkovskaya, and C. L. Watkins, "Repetitive Task Training for Improving Functional Ability after Stroke: A Major Update of a Cochrane Review," *Stroke*, vol. 48, no. 4, pp. e102–e103, 2017.

[2] J. Bo Nielsen, M. Willerslev-Olsen, L. Christiansen, J. Lundbye-Jensen, and J. Lorentzen, "Science-based neurorehabilitation: Recommendations for neurorehabilitation from basic science," *Journal of Motor Behavior*, vol. 47, no. 1, pp. 7–17, 2015.

[3] R. A. Gopura, D. S. Bandara, K. Kiguchi, and G. K. Mann, "Developments in hardware systems of active upper-limb exoskeleton robots: A review," *Robotics and Autonomous Systems*, vol. 75, no. October, pp. 203–220, 2016.

[4] T. Proietti and V. Crocher, "Upper-Limb Robotic Exoskeletons for Neurorehabilitation : A Review on Control Strategies," vol. 9, pp. 4–14, 2016.

[5] V. Klamroth-Marganska, J. Blanco, K. Campen, A. Curt, V. Dietz, T. Ettlin, M. Felder, B. Fellinghauer, M. Guidali, A. Kollmar, A. Luft, T. Nef, C. Schuster-Amft, W. Stahel, and R. Riener, "Three-dimensional, task-specific robot therapy of the arm after stroke: A multicentre, parallel-group randomised trial," *The Lancet Neurology*, vol. 13, no. 2, pp. 159–166, 2014.

[6] M. Ferreira, M. Em, A. Chaves, F. Ma, C. Oliveira, A. Maria, C. Bruno, and S. Vimieiro, "Effectiveness of robot therapy on body function and structure in people with limited upper limb function : A systematic review and meta-analysis," *PlosOne*, pp. 1–21, 2018.

[7] R. C. Loureiro, W. S. Harwin, K. Nagai, and M. Johnson, "Advances in upper limb stroke rehabilitation: A technology push," *Medical and Biological Engineering and Computing*, vol. 49, no. 10, pp. 1103–1118, 2011.

[8] A. Otten, C. Voort, A. Stienen, R. Aarts, E. Van Asseldonk, and H. Van Der Kooij, "LIMPACT:A Hydraulically Powered Self-Aligning Upper Limb Exoskeleton," *IEEE/ASME Transactions on Mechatronics*, vol. 20, no. 5, pp. 2285–2298, 2015.

[9] T. Nef, M. Guidali, and R. Riener, "ARMin III arm therapy exoskeleton with an ergonomic shoulder actuation," *Applied Bionics and Biomechanics*, vol. 6, no. 2, pp. 127–142, 2009.

[10] B. Kim and A. D. Deshpande, "An upper-body rehabilitation exoskeleton Harmony with an anatomical shoulder mechanism: Design, modeling, control, and performance evaluation," *The International Journal of Robotics Research*, vol. 36, no. 4, pp. 414–435, 2017.

[11] F. Just, Ö. Özen, P. Bösch, H. Bobrovsky, V. Klamroth-Marganska, R. Riener, and G. Rauter, "Exoskeleton transparency: feed-forward compensation vs. disturbance observer," *at - Automatisierungstechnik*, vol. 66, no. 12, pp. 1014–1026, 2018.

[12] J. Rosen, J. C. Perry, N. Manning, S. Burns, and B. Hannaford, "The human arm kinematics and dynamics during daily activities - Toward a 7 DOF upper limb powered exoskeleton," *2005 International Conference on Advanced Robotics, ICAR '05, Proceedings*, vol. 2005, no. July, pp. 532–539, 2005.

[13] T. Horibe, E. T. B, and R. B. Gillespie, "Comparing Series Elasticitz and Admittance Control for Haptic Rendering," *EuroHaptics 2016*, vol. 5024, pp. 240–250, 2016.

[14] H. Vallery, J. Veneman, E. van Asseldonk, R. Ekkelenkamp, M. Buss, and H. van Der Kooij, "Compliant actuation of rehabilitation robots," *IEEE Robotics and Automation Magazine*, vol. 15, no. 3, pp. 60–69, 2008.

[15] T. L. Brooks, "Telerobotic response requirements," *Systems, Man and Cybernetics, 1990. Conference Proceedings., IEEE International Conference on*, pp. 113–120, 1990.

[16] S. Namdari, G. Yagnik, D. D. Ebaugh, S. Nagda, M. L. Ramsey, G. R. Williams, and S. Mehta, "Defining functional shoulder range of motion for activities of daily living," *Journal of Shoulder and Elbow Surgery*, vol. 21, no. 9, pp. 1177–1183, 2012.

[17] D. J. Magermans, E. K. J. Chadwick, H. E. J. Veeger, and F. C. T. Van Der Helm, "Requirements for upper extremity motions during activities of daily living," *Clinical Biomechanics*, vol. 20, no. 6, pp. 591–599, 2005.

[18] D. H. Gates, L. S. Walters, J. Cowley, J. M. Wilken, and L. Resnik, "Range of motion requirements for upper-limb activities of daily living," *American Journal of Occupational Therapy*, vol. 70, no. 1, 2016.

[19] G. Wu, F. C. T. Van der Helm, H. E. J. Veeger, M. Makhsous, P. V. Roy, C. Anglin, J. Nagels, A. R. Karduna, K. McQuade, X. Wang, F. W. Werner, and B. Buchholz, "ISB recommendation on definitions of joint coordinate systems of various joints for the reporting of human joint motioN, Part II: shoulder, elbow, wrist and hand," *Journal of Biomechanics*, vol. 38, no. 5, pp. 981–992, may 2005.

[20] J. Y. Hogrel, C. A. Payan, G. Ollivier, V. Tanant, S. Attarian, A. Couillandre, A. Dupeyron, L. Lacomblez, V. Doppler, V. Meininger, C. Tranchant, J. Pouget, and C. Desnuelle, "Development of a French Isometric Strength Normative Database for Adults Using Quantitative Muscle Testing," *Archives of Physical Medicine and Rehabilitation*, vol. 88, no. 10, pp. 1289–1297, 2007.

[21] T. Nef, R. Riener, R. Müri, and U. P. Mosimann, "Comfort of two shoulder actuation mechanisms for arm therapy exoskeletons: A comparative study in healthy subjects," *Medical and Biological Engineering and Computing*, vol. 51, no. 7, pp. 781–789, 2013.

[22] J. Pratt, B. Krupp, and C. Morse, "Series elastic actuators for high fidelity force control," *Industrial Robot: An International Journal*, vol. 29, no. 3, pp. 234–241, 2002.

[23] M. Hutter, C. Gehring, D. Jud, A. Lauber, C. D. Bellicoso, V. Tsounis, J. Hwangbo, P. Fankhauser, M. Bloesch, R. Diethelm, and S. Bachmann, "ANYmal - A Highly Mobile and Dynamic Quadrupedal Robot," *submitted to IEEE/RSJ Intenational Conference on Intelligent Robots and Systems (IROS)*, 2016.

[24] M. Hutter, K. Bodie, A. Lauber, and J. Hwangbo, "EP16181251 - Joint unit, joint system, robot for manipulation and/or transportation, robotic exoskeleton system and method for manipulation and/or transportation," 2016.

[25] J. S. Sehrawat and R. K. Pathak, "Variability in anatomical features of human clavicle: Its forensic anthropological and clinical significance," *Translational Research in Anatomy*, vol. 3-4, pp. 5–14, 2016.

[26] C. Dario Bellicoso, C. Gehring, J. Hwangbo, P. Fankhauser, and M. Hutter, "Perception-less terrain adaptation through whole body control and hierarchical optimization," in *IEEE-RAS International Conference on Humanoid Robots*, 2016, pp. 558–564.

[27] A. H. Stienen and A. Q. Keemink, "Visualization of shoulder range of motion for clinical diagnostics and device development," *IEEE International Conference on Rehabilitation Robotics*, vol. 2015-Septe, pp. 816–821, 2015.